

Exciton-Selective Phonon Coupling in a Lead Halide Perovskite

Pradeepa H L,^{1,*} Sagnik Chatterjee,¹ Sayantan Patra,¹ Swapneswar Bisoi,¹ Saqlain Mushtaq,¹ Hardeep,² Akshay Singh,² Ashish Arora,¹ and Atikur Rahman^{1,†}

¹*Department of Physics, Indian Institute of Science Education and Research(IISER), Pune 411008, India*

²*Department of Physics, Indian Institute of Science, Bangalore 560012, India*

Exciton-phonon interactions govern the optical response of semiconductors, yet disentangling multiple coupling channels in lead halide perovskites remains challenging. We investigate CsPbBr_3 microcrystals using photoluminescence, Raman and reflectance spectroscopy at low temperature, revealing the simultaneous presence of high-energy and Rashba excitons, each accompanied by distinct phonon replica series. High-energy exciton replicas are uniquely spaced by approximately 9 meV, whereas Rashba exciton replicas exhibit a characteristic approximately 6 meV spacing, indicating the specificity of the exciton-phonon coupling. Unsupervised machine learning applied to a large low-temperature photoluminescence dataset reveals these replica features are prevalent. With increasing temperature, replica features broaden and merge, evolving into a dominant longitudinal optical phonon coupling regime at room temperature. This work establishes direct spectroscopic evidence for concurrent, exciton-specific phonon coupling within a single material, offering new pathways to engineer light-matter interactions for optoelectronic and phonon-photon-based quantum device applications.

Excitons, bound electron-hole pairs, are key quasiparticles shaping the optical properties of semiconductors and their interaction with phonons profoundly influences spectral characteristics and energy dissipation, making the elucidation of these mechanisms crucial for the rational design of next-generation materials [1, 2]. Due to their soft crystal lattices, lead-halide perovskites (APbX_3 ; A = Cs, MA, etc.; X = Cl, Br, I) exhibit strong exciton-phonon coupling [3, 4]. In addition, they possess extraordinary optical properties, including a high photoluminescence (PL) quantum yield, strong light absorption, long carrier lifetimes, and a widely tunable bandgap. Together, these remarkable features make them both fundamentally interesting and highly promising for optoelectronic and energy applications [5, 6].

Precise control of exciton-phonon interactions in these materials is pivotal for advancing optoelectronics, from solar cells to quantum computing platforms[5, 7]. Amidst these materials, CsPbBr_3 is highly studied for its intriguing optical response[1, 5, 7–10], but its fundamental properties, especially the nature of excitonic states and their coupling with phonons, remain debatable [1, 2, 6, 11–13]. The existence and precise nature of Rashba excitons are of particular interest[7, 14–19], with origins attributed to polar fluctuations and lattice distortions[15, 20, 21]. Identifying the spectroscopic fingerprints of these debated excitons and their coupling is paramount. Despite extensive effort, the direct and simultaneous observation of multiple excitonic species, each with a distinct phonon replica series, is scarce[17, 19, 21–26]. Specifically, the interplay between high-energy excitons and Rashba excitons and their coupling to different phonon modes remains unresolved in a single material system.

In this article, we intend to provide direct evidence, not only of the debated Rashba exciton in CsPbBr_3 , but also for its intriguing and distinct phonon coupling behaviour, offering a critical contribution to this long-standing discussion.

Using synergistic low temperature PL, reflectance, and Raman spectroscopy on CsPbBr_3 microcrystals, we reveal the coexistence of high-energy and Rashba excitons. Crucially, each exciton exhibits an equispaced phonon replica series attributed to coupling to distinct phonon modes an uncommon observation in microcrystals, where coupling typically diminishes[22, 27, 28]. Their temperature evolution uncovers a crossover to a dominant high-energy longitudinal optical (LO) phonon coupling regime at room temperature. We statistically confirmed the frequent occurrence of these replica features using the k-means clustering algorithm on 260 PL spectra. These findings offer fundamental understanding to control exciton-phonon dynamics for advanced opto-electronics and phonon-photon based quantum devices[29].

We synthesized CsPbBr_3 perovskite samples using a new near-room-temperature solvothermal method . An alcohol-based solvent enables controlled growth of large-area, highly crystalline structures under mild conditions[30](see SI). Fig. 1 presents an overview of the morphological and optical characteristics of the CsPbBr_3 sample. Optical and wide-field PL images at room temperature show strong emission with 405 nm excitation (Fig. 1 (a) and (b)). Atomic force microscopy (AFM) shows the crystal height ranges from 200 nm to 900 nm Fig. 1 (c) (SI S2). The low-temperature (77 K) Raman spectrum exhibits characteristic CsPbBr_3 single crystal peaks (Fig. 1 (d)). Strong phonon peaks are observed at 9 meV (P_2) and 10 meV (P_3), attributed to octahedra distortions[31]. A less intense peak at 16 meV relates to Pb-Br bond stretching[13], and a longitudinal optical (LO) phonon peak is observed at 38 meV[3, 32].

At 77 K, upon excitation, we observed multiple clearly resolved emission peaks (Figure 2 a-c), which can be attributed to different excitonic species with various recombination pathways. Interestingly, we observe that the first peak (FX) at the highest energy is not of the highest intensity. There exist multiple lower energy peaks, among which the peak \sim 14–20 meV below the FX is of the highest intensity. Upon careful observation of multiple samples, the highest intensity peak is found to consist of one, two or three closely spaced peaks. Fig 2 (a-c) shows the PL of the samples, which exhibits a sin-

* hl.pradeepa@acads.iiserpune.ac.in

† atikur@iiserpune.ac.in

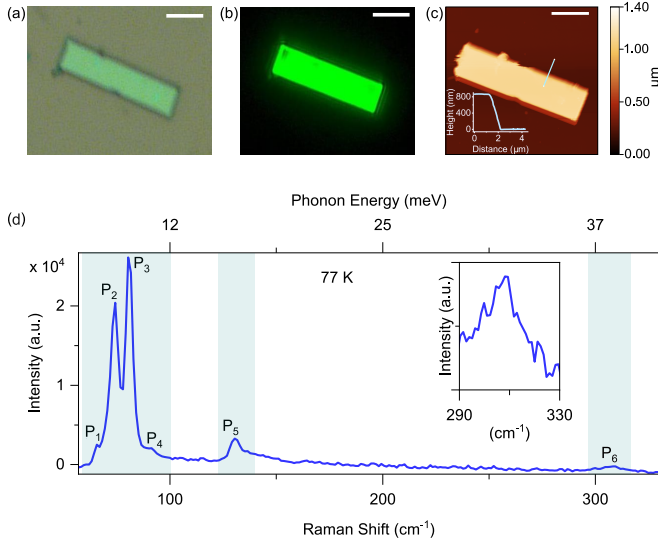


FIG. 1: Morphological and optical characterization of CsPbBr_3 sample. (a) Optical image and (b) Wide-field PL image of the CsPbBr_3 sample, demonstrating strong emission. (c) Atomic force microscopy (AFM) image and corresponding height profile(inset), which shows a sample height of $\sim 0.83 \mu\text{m}$. (Scale bar: 5 μm .) (e) Raman spectra at 77 K, exhibiting phonon peaks at 8 meV (P_1), 9 meV (P_2), 10 (P_3) and 11 meV (P_4), with an additional weaker peaks at 16 meV (P_5) and 38 meV. Inset is a magnified view of the peak P_6 .

gle, double (RX' and RX'') and triple (RX' , RX'' and RX''') split in the highest intensity emission peak. These single, double, and triple emission features were observed in multiple samples. Fig 2 (d-f) shows typical single, double (with energy separation Δ_1) and triple (with energy separations Δ_2 and Δ_3) peak-split of the peaks in different samples. The distribution of these splittings Δ_1 , Δ_2 and Δ_3 across samples showing these values lies in the range of $\sim 1\text{-}2$ meV (Fig 2 (g-i)). This signature peak-split has previously been associated with Rashba exciton in various CsPbX_3 crystals [7, 22, 33–35]. We assign these peaks to originate from Rashba spin-orbit split triplet [7, 15, 21, 33] and define the mean position of the splitted peaks as Rashba exciton (RX). We estimate the Rashba coupling strength parameter α from the expression:

$$\alpha^2 = \frac{2\hbar^2(E_{\text{FX}} - E_{\text{RX}})}{m^*} \quad (1)$$

where, m^* is the effective mass of exciton (0.126 m_0)[36]. The estimated values of $\alpha \sim 1.39$, close to the value previously reported[21]. Apart from the Rashba peaks, multiple distinct peaks were noticed in lower energy sides; these peaks are likely to involve trions, biexcitons, defect-bound excitons, or phonon replicas[15].

Fig 2 (j) shows a colour map of PL of the sample showing double split Rashba peaks at different powers at 77 K, the peaks showing no energy shift with varying power. Fig 2 (k) shows the normalised PL at different powers, where we observed no changes in the position and relative intensity. These observations suggest the absence of emission from de-

fect states, and the lower energy peak intensities scale as the highest intensity peak, hinting towards the same excitonic origin of those peaks[37]. It is important to note that metal halide perovskites, including CsPbBr_3 , are known to have defect tolerance[38].

To study the origin of the emissions other than FX and RX, we further analysed the PL and reflectance contrast spectra. Fig 3 (a) shows the PL spectrum. In addition to the FX and RX, the other distinct peaks are found, and we noticed that all these peaks, including the FX and RX, can be grouped into two distinct sets of peaks, with the highest energy peak of the set being the FX and RX. The peaks within the sets exhibit an equally spaced characteristic. These equally separated peaks can be assigned as phonon replicas of FX and RX (SI S3).

First, we will discuss the replicas of FX. In Fig 3 (a), the peaks indicated by broken blue lines, FX, F_1 , F_2 and F_3 exhibit an approximately equal spacing of $\Delta E_1 \sim 9\text{-}10$ meV. We assign these peaks to phonon replicas of the first exciton. Additionally, another peak (F'_1) was observed, separated by around 11 meV below the FX. S3 Table 1 in the Supplementary Information summarises the observed peaks, their energies, and their energy differences relative to the FX.

The Rashba peak exhibits two main peaks: 2.352 eV and 2.350 eV. Interestingly, these two primary Rashba peaks also display phonon replicas with equal energy spacing, similar to what is observed for FX. To simplify our discussions ahead, we have assigned the mean position of the RX replica doublets as R_1 , R_2 , R_3 , and R_4 . The energy separation of these replicas with respect to the mean of the main Rashba peak RX is indicated by the purple lines in Fig 3 (a) is ΔE_2 . It is found that $\Delta E_2 \sim 5\text{-}6$ meV. S3 Table 2 in Supplementary Information provides a summary of these peaks, their energies, and their energy differences relative to the Rashba exciton position RX. The inset in Fig. 3 (a) shows the variation of $\Delta E = (E_{\text{ZPL}} - E_n)/n$ with the replica number(n), where E_{ZPL} and E_n corresponds to the energy of the zero phonon line (ZPL), i.e. $\text{FX}(\text{RX})$ and the ‘n’-th phonon replica ($n = 1, 2, 3, \text{etc.}$) of $\text{FX}(\text{RX})$. This summarises the calculated energy separations for all the replicas. For the ‘n’-th phonon replica of FX and RX, ΔE is found to be nearly constant and with mean $\Delta E_1 \sim 9.3 \pm 0.4$ meV and $\Delta E_2 \sim 5.6 \pm 0.2$ meV.

Fig 3 (b) (blue curve) displays the differential reflectance (DR) spectrum calculated from the reflected signal from the sample (R_{sample}) and the substrate ($R_{\text{substrate}}$) as,

$$DR = (R_{\text{sample}} - R_{\text{substrate}})/R_{\text{substrate}} \quad (2)$$

For a clearer picture, the Differential Reflectance (DR) was simulated using a multi-Lorentz oscillator model, which agrees well with experimental data[39]. The simulated curves, shown as a green curve in Fig 3 (b), are in good agreement with the experimental data. To better identify transition levels, the First Derivative of Reflectance (DDR) was plotted as shown in Fig 3 (c) (blue curve). Each dip in the DDR corresponds to a transition energy, blueshifted by $\sim 1\text{-}2$ meV compared to PL peaks. The FX transition level and its three phonon replicas are clearly seen with an energy separation ΔE_1 of ~ 9 meV, matching PL data. The Rashba split peaks (RX' and RX'') are distinct minima with a ~ 2 meV separa-

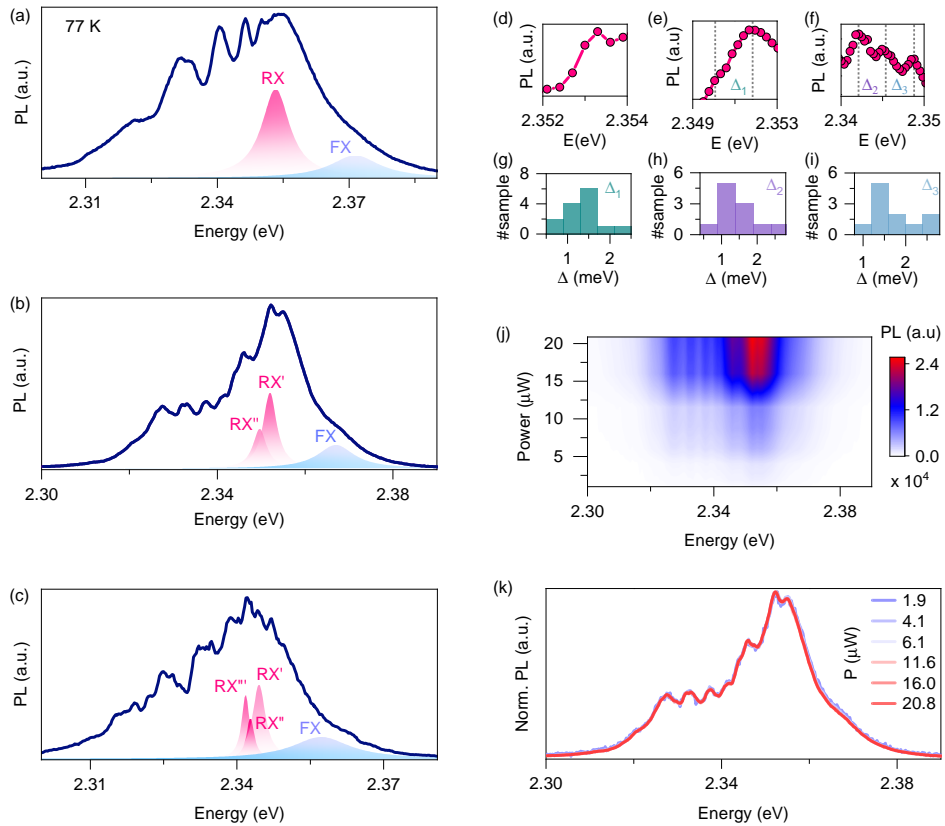


FIG. 2: Low-temperature PL and power dependence. PL spectra at 77 K, multiple distinct emission peaks are observed, including the high energy first exciton (FX) and Rashba exciton (RX). (a) Shows the PL of the sample which exhibit single Rashba emission. (b) PL of the sample with double Rashba emission (RX' and RX''), which appear as a peak and a hump in the spectra. (c) shows the PL of the sample where Rashba peak consists of three peaks (RX', RX'' and RX'''). (d-e) The single, double (with energy separation Δ_1) and triple (with energy separations Δ_2 and Δ_3) Rashba emission respectively in different samples. (g-i) Δ_1 , Δ_2 , and Δ_3 distribution in different number of samples. (j) Colour map of PL intensity as a function of excitation power, showing no significant energy shift with varying power. (k) Normalised PL spectra at different excitation powers showing the low energy peaks scale like the highest intensity peak.

tion, strengthening their assignment. RX replicas are also observed, separated by ~ 5 meV, with the second overlapping the FX's third replica, similar to PL.

The temperature dependence of the PL and Raman spectra (Fig 3 (d,e)) provides insight into the phonon replicas. PL peak energy positions (Fig 3 (d)) maintain an approximately equal separation up to 120 K. The Raman spectra (Fig 3 (e)) show stable strong peaks around 9 meV and 10 meV, with their positions largely unchanged across this temperature range. This signature for these phonon modes, as well as for the lower energy phonon modes, is also previously reported in this temperature window [31, 40]. This stability in both the PL energy separation and Raman peak positions supports the assignment of these features as exciton-phonon replicas [37, 41, 42].

Fig 4 (a,b) show the normalised PL spectra of samples showing single split and triple split Rashba peaks, respectively, as a function of the energy separation from E_{FX} . The single split case shows five FX and five RX phonon replicas, with some overlaps observed (e.g., F_3 with R_2). The triple

split case shows four FX and five RX replicas, also with overlaps attributed to accidental energy matching. In both cases, the phonon replica separations are consistent: ΔE_1 is ~ 9 -10 meV and ΔE_2 is ~ 5 -6 meV. Since these separations remain unchanged across samples of different thicknesses, an interference effect is unlikely. Fig 4 (c) indicates the mean ΔE_1 and ΔE_2 for all the samples. The average phonon energies, $\Delta E_1 \sim 9.4 \pm 0.2$ meV and $\Delta E_2 \sim 5.6 \pm 0.1$ meV, shown in the shaded grey area are close to the known phonon bands [3, 23, 31, 43].

The Huang-Rhys(HR) factor is the standard observable for quantifying the exciton-phonon coupling strength. This factor quantifies the intensity of phonon side bands relative to the main zero-phonon line [27]. Single phonon HR factor (S_9^1) for a phonon mode with energy ν meV is estimated for FX and RX [44]. For FX S_9^1 ranges from 1.6 to 3.6 and for RX S_6^1 ranges from 0.75 to 0.94 in the samples studied. This results in a clear contrast with the reported decrease of the HR factor with increasing crystal size [22, 27]. Notably, the FX S_9^1 is, to the best of our knowledge, the highest reported single phonon

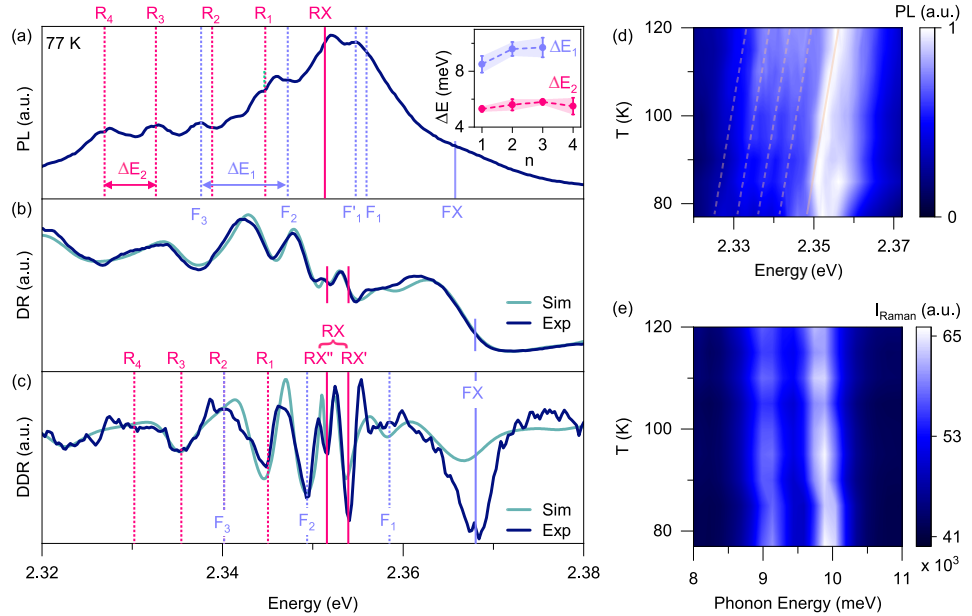


FIG. 3: Low-temperature (77 K) correlated PL, reflectance, and Raman spectra. (a) PL spectra showing equally separated phonon replica peaks of the FX and RX, with an additional peak F'_1 . The inset shows the replica number (n) vs. ΔE plot for the FX and the RX replicas. (b) Differential reflectance (DR) spectrum. The teal curve shows the simulated DR spectra. (c) First derivative of the differential reflectance (DDR) spectrum. The dips in the DDR correspond to a transition energy, where equally separated phonon replicas of FX and RX are observed. (d) Temperature-dependent PL energy separation, showing a constant energy separation across the given temperature range. (e) Temperature-dependent Raman spectra, exhibiting two strong peaks around 9 meV and 10 meV, exhibit nearly constant intensity and energy within the given temperature regime.

HR factor in CsPbBr_3 microcrystals. Pronounced exciton-phonon coupling has primarily been observed in nanocrystals of perovskites at exceedingly low temperatures, its strength tending to diminish in larger crystals [22, 27, 28]. However, our observations suggest the presence of this coupling in microcrystals, which is quite uncommon; this invites reexamination of the established view that particle size dictates exciton-phonon behaviour in lead halide perovskites. We have also noticed the existence of F'_1 approximately below 11 meV from the FX for these two samples.

Our observations confirm two key features: the existence of a low-energy Rashba exciton and distinct phonon replicas for both high-energy and Rashba excitons in CsPbBr_3 microcrystals. To explore the microscopic origins, we examine the crystal structure as shown Fig 4 (d). Bending of the Pb-Br-Pb bond with a subtle displacement of the Cs^+ cation within the unit cell is reported in CsPbBr_3 nanocrystals[45]. This displacement of the Cs^+ cation within the orthorhombic unit cell breaks inversion symmetry[30], which can induce a strong Rashba spin-orbit interaction. Additionally, octahedral polar fluctuations or surface termination can cause the dynamic structural distortion necessary for the Rashba effect[15, 20, 21, 46–49].

Phonon replicas manifest as distinct signatures in both DR and PL spectra[39, 50, 51], granting us an opportunity to explore exciton-phonon coupling in this system. In this study, we observed phonon replicas as equally separated lines with energy separations of ~ 6 meV and ~ 9 meV. As we previ-

ously discussed, Raman spectra revealed prominent phonon modes within the energy band between 8-12 meV at 77 K. Alongside this dominant phonon mode, other lower-energy phonon modes, specifically between 5-7 meV, are observed in CsPbBr_3 [3, 20, 22, 23, 31, 43]. In our study, the phonon modes within the 8-12 meV band are associated with the high energy exciton, leading to the prominent high energy exciton phonon replicas that we observe in both DR and PL spectra. The lower-energy phonon modes in the 5-7 meV band remain crucial in the formation of Rashba exciton replicas. These phonon modes are related to the bending of the Pb-Br-Pb bonds[2, 4, 22, 52, 53]. As we previously discussed, a displacement of the Cs^+ cation with the Pb-Br-Pb bond bending containing heavy atoms like Pb gives rise to a strong Rashba spin-orbit coupling effect in CsPbBr_3 . Thus, these low-frequency modes, through local structural distortions, can create a deformation potential which may induce exciton-phonon interaction,[2, 54, 55] leading towards phonon replicas in the DR and emission spectra. Fig 4 (e) represents a schematic summary of the proposed model for low-temperature phonon replicas of FX and RX. The F'_1 is probably due to the coupling of the 11 meV phonon mode with FX.

To understand temperature's effect on exciton interactions, we analyzed the evolution of PL spectra from 77 K to 300 K. As temperature rises, thermal broadening causes the distinct low energy phonon replicas to merge into a single, broad peak around 150 K[37, 56]. This peak further merges with the Rashba exciton peak near 190 K, forming a dominant peak

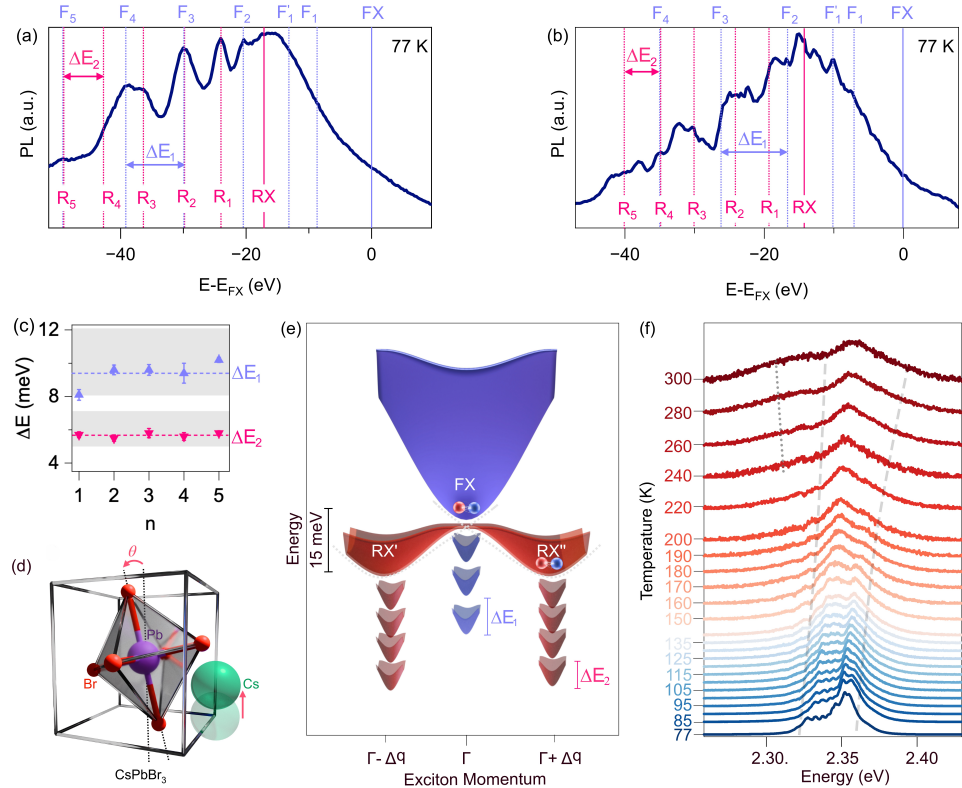


FIG. 4: Structural and recombination pathways, with samples comparison. (a) and (b) show normalised PL spectra of samples showing single split and triple split Rashba peaks, as a function of the energy separation of the RX and all replicas with respect to FX, respectively. (c) n vs mean ΔE for FX and RX of the samples. The dotted lines indicate the mean phonon energy involved in the replica generation process ($\Delta E_1 \sim 9.4$ meV and $\Delta E_2 \sim 5.6$ meV). The shaded area indicates the available phonon energy bands. (d) Crystal structure of CsPbBr_3 . The slight displacement of the Cs^+ cation within the unit cell leads to its occupation at two distinct positions. The $\text{Pb}-\text{Br}-\text{Pb}$ bond also tilts by an angle θ due to this displacement. (e) Schematic illustration of the various exciton levels, including the FX, RX, and their respective phonon replicas. The discrete replica states are depicted lying under their corresponding energy valleys. (f) Temperature evolution of PL spectra of the sample showing a double-split Rashba peak. With increasing temperature, sharp phonon replica features broaden and merge, evolving into a single peak with a hump at room temperature (enclosed by dashed grey lines). The dotted grey line (240-300 K) shows the emergence of the high-temperature phonon replica region.

that persists up to 300 K (enclosed by dashed grey lines). Interestingly, an additional, lower energy broad peak emerges at 240 K, and its relative intensity increases with temperature (indicated by dotted grey lines). At high temperatures, the PL spectrum resolves into multiple peaks (see SI S5), with the Rashba splitting (~ 24 meV) increasing [15]. As lower energy Raman modes vanish[31],(see SI S6) a prominent $\sim 58 \pm 1.3$ meV phonon replica separation emerges near room temperature, attributed to the combination of the 19 meV and 38 meV Raman active modes[55]. These findings demonstrate a temperature driven crossover in phonon replicas, from low energy phonon dominance at low temperatures to LO phonon dominance at higher temperatures, necessitating further theoretical investigation into lattice dynamics, anharmonicity, and screening effects[44].

To better understand the variations in the spectral signatures, we performed a statistical analysis on low-temperature (77 K) normalised PL spectra from 260 samples using principal component analysis (PCA) and k-means clustering. The

k-means analysis identified three distinct clusters: C1 (blue), C2 (orange), and C3 (grey), as shown in Fig 5 (a) (SI S7). Most samples fall into clusters C1 or C2, with only a small number of samples exhibiting the emission signatures of cluster C3. This is evident from the high-density regions of C1 and C2 in Fig 5(a) and the percentage distribution for each cluster shown in Fig 5 (b). The mean spectrum for each cluster is shown in Fig 5 (c), where highlighted regions indicate the standard deviation. Notably, the mean spectra for C1 and C2 show low intra-cluster variation. In contrast, the mean spectrum for C3, centred at a higher energy, exhibits comparatively high variation. Therefore, C3 represents a cluster of outliers with higher-energy emissions. To illustrate the nature of the emission, Fig 5 (d) presents two representative spectra from each cluster. The spectra in C1 and C2 prominently feature FX, RX, and their phonon replicas, and the relative strength of these replicas distinguishes the two clusters. In C1, the phonon replica region is lower in intensity, whereas in C2, the replicas are significantly stronger, with numerous closely

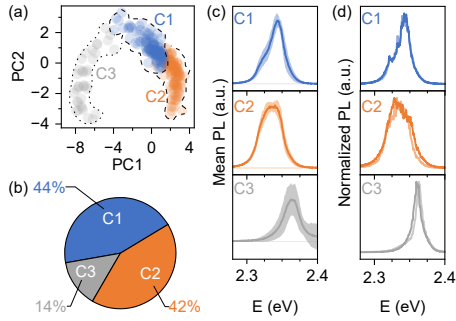


FIG. 5: Statistical study of the emission characteristics for 260 samples. (a) Principal component scatter plot and k-means clustering of the emission lineshapes. The emission lineshape is classified into three clusters: C1 (blue), C2 (orange) and C3 (grey). C1 and C2 show the highest density in the scattered plot, referring to the most probable lineshapes. (b) Percentage distribution of the clusters. (c) Mean emission curve of clusters C1 (top panel), C2 (middle panel) and C3 (bottom panel) (in solid line). The highlighted region in each panel shows the variation of the spectra within the cluster across the mean spectra. (d) Two representative spectra from clusters C1 (top panel), C2 (middle panel) and C3 (bottom panel).

spaced peaks merging to form a broad emission band (SI Figure S7e). In conclusion, most of the samples studied show emission dominated by FX, RX, and their respective phonon replicas.

In summary, our comprehensive study on CsPbBr_3 microcrystals reveals a rich, complex optical response, demonstrating the unambiguous observation of coexisting high-energy and Rashba excitons, each exhibiting a distinct phonon replica series that highlights multiple exciton–phonon coupling channels and challenges established views on particle-size dependence. Furthermore, the coupling is dynamic, showing a progressive merging of replicas with rising temperature and a crossover to a dominant longitudinal optical (LO) phonon coupling regime at room temperature, demonstrating adaptability in their interaction pathways. The intrinsic, exciton selective coupling enables a materials-by-design paradigm for quantum control using perovskites.

HLP acknowledges funding support from the National Mission on Interdisciplinary Cyber-Physical Systems (NM-ICPS) of the DST, Government of India, through the I-HUB Quantum Technology Foundation, Pune, India. SC thanks the Prime Minister's Research Fellowship, Govt. of India, for providing a research fellowship. AR acknowledges funding support from DST SERB grant no. CRG/2021/005659. AS acknowledges funding from Department of Science and Technology Nanomission CONCEPT grant (NM/TUE/QM-10/2019). AA acknowledges financial support from the following projects funded by the Government of India: NM-ICPS of the DST through the I-HUB Quantum Technology Foundation (Pune, India), Project No. CRG/2022/007008 of SERB, MoE-STARS project No. MoE-STARS/STARS-2/2023-0912, CEFIPRA CSRP Project No. 7104-2, and DST National Quantum Mission project No. DST/QTC/NQM/QMD/2024/4 (G).CRG/2021/005659.

[1] M. Baranowski and P. Plochocka, Excitons in metal-halide perovskites, *Advanced Energy Materials* **10**, 1903659 (2020).

[2] Y. Yamada and Y. Kanemitsu, Electron-phonon interactions in halide perovskites, *NPG Asia Materials* **14**, 48 (2022).

[3] C. M. Iaru, A. Brodu, N. J. J. van Hoof, S. E. T. ter Huurne, J. Buhot, F. Montanarella, S. Buhbut, P. C. M. Christianen, D. Vanmaekelbergh, C. de Mello Donega, J. G. Rivas, P. M. Koenraad, and A. Y. Silov, Fröhlich interaction dominated by a single phonon mode in cspbbr_3 , *Nature communications* **12**, 5844 (2021).

[4] K. Cho, T. Yamada, H. Tahara, T. Tadano, H. Suzura, M. Saruyama, R. Sato, T. Teranishi, and Y. Kanemitsu, Luminescence fine structures in single lead halide perovskite nanocrystals: size dependence of the exciton–phonon coupling, *Nano Letters* **21**, 7206 (2021).

[5] Q. A. Akkerman, G. Rainò, M. V. Kovalenko, and L. Manna, Genesis, challenges and opportunities for colloidal lead halide perovskite nanocrystals, *Nature materials* **17**, 394 (2018).

[6] A. K. Poonia, P. Salunkhe, A. Nag, and K. V. Adarsh, Emerging collective quantum phenomena of excitons in metal-halide perovskites, *MRS Bulletin* **49**, 862 (2024).

[7] M. A. Becker, R. Vaxenburg, G. Nedelcu, P. C. Sercel, A. Shabaev, M. J. Mehl, J. G. Michopoulos, S. G. Lambrakos, N. Bernstein, J. L. Lyons, T. Stöferle, R. F. Mahrt, M. V. Kovalenko, D. J. Norris, G. Rainò, and A. L. Efros, Bright triplet excitons in caesium lead halide perovskites, *Nature* **553**, 189 (2018).

[8] S. S. Kharintsev, E. I. Battalova, I. A. Matchenya, A. G. Nasibulin, A. A. Marunchenko, and A. P. Pushkarev, Extreme electron–photon interaction in disordered perovskites, *Advanced Science* **2405709** (2024).

[9] L. Wu, K. Chen, W. Huang, Z. Lin, J. Zhao, X. Jiang, Y. Ge, F. Zhang, Q. Xiao, Z. Guo, Y. Xiang, J. Li, Q. Bao, and H. Zhang, Perovskite cspbx_3 : a promising nonlinear optical material and its applications for ambient all-optical switching with enhanced stability, *Advanced Optical Materials* **6**, 1800400 (2018).

[10] K. Wei, Z. Xu, R. Chen, X. Zheng, X. Cheng, and T. Jiang, Temperature-dependent excitonic photoluminescence excited by two-photon absorption in perovskite cspbbr_3 quantum dots, *Optics letters* **41**, 3821 (2016).

[11] J. Fu, S. Ramesh, J. W. Melvin Lim, and T. C. Sum, Carriers, quasi-particles, and collective excitations in halide perovskites, *Chemical Reviews* **123**, 8154 (2023).

[12] M. Baranowski, K. Galkowski, A. Surrente, J. Urban, Ł. Kłopotowski, S. Maćkowski, D. K. Maude, R. Ben Aich, K. Boujdaria, M. Chamorro, *et al.*, Giant fine structure splitting of the bright exciton in a bulk mapbbr_3 single crystal, *Nano Letters* **19**, 7054 (2019).

[13] A. S. Abbas, B. C. Li, R. D. Schaller, V. B. Prakapenka, S. Chariton, D. Bian, G. S. Engel, and A. P. Alivisatos, Efficient up-conversion in cspbbr_3 nanocrystals via phonon-driven exciton-polaron formation, *Nature Communications* **16**, 10.1038/s41467-025-60992-y (2025).

[14] J. A. Steele, P. Puech, B. Monserrat, B. Wu, R. X. Yang, T. Kirchartz, H. Yuan, G. Fleury, D. Giovanni, E. Fron, et al., Role of electron–phonon coupling in the thermal evolution of bulk rashba-like spin-split lead halide perovskites exhibiting dual-band photoluminescence, *ACS energy letters* **4**, 2205 (2019).

[15] B. Wu, H. Yuan, Q. Xu, J. A. Steele, D. Giovanni, P. Puech, J. Fu, Y. F. Ng, N. F. Jamaludin, A. Solanki, S. Mhaisalkar, N. Mathews, M. B. J. Roeffaers, M. Grätzel, J. Hofkens, and T. C. Sum, Indirect tail states formation by thermal-induced polar fluctuations in halide perovskites, *Nature communications* **10**, 484 (2019).

[16] M. Kepenekian and J. Even, Rashba and dresselhaus couplings in halide perovskites: Accomplishments and opportunities for spintronics and spin–orbitronics, *The Journal of Physical Chemistry Letters* **8**, 3362 (2017).

[17] M. Isarov, L. Z. Tan, M. I. Bodnarchuk, M. V. Kovalenko, A. M. Rappe, and E. Lifshitz, Rashba effect in a single colloidal cspbbr3 perovskite nanocrystal detected by magneto-optical measurements, *Nano letters* **17**, 5020 (2017).

[18] M. Dendebera, Y. Chornodolskyy, R. Gamernyk, O. Antonyak, I. Pashuk, S. Myagkota, I. Gnilitskyi, V. Pankratov, V. Vistovskyy, V. Mykhaylyk, M. Grinberg, and A. Voloshinovskii, Time resolved luminescence spectroscopy of cspbbr3 single crystal, *Journal of Luminescence* **225**, 117346 (2020).

[19] M. Dendebera, T. Malyi, A. Zhyshkovych, Y. Chornodolskyy, A. Pushak, R. Gamernyk, O. Antonyak, T. Demkiv, V. Vistovskyy, and A. Voloshinovskii, Temperature behavior of the near band edge luminescence in cspbbr3 single crystal and nanoparticle ensemble, *Optical Materials: X* **16**, 100208 (2022).

[20] O. Yaffe, Y. Guo, L. Z. Tan, D. A. Egger, T. Hull, C. C. Stoumpos, F. Zheng, T. F. Heinz, L. Kronik, M. G. Kanatzidis, et al., Local polar fluctuations in lead halide perovskite crystals, *Physical review letters* **118**, 136001 (2017).

[21] W. Yao, S. Lan, Y. Wang, Q. Feng, Z. Yang, G. Nan, Q. Xiong, and D. Li, Crystal-phase-engineered rashba indirect exciton emission in cspbbr3 single crystals, *The Journal of Physical Chemistry Letters* **16**, 3799 (2025).

[22] K. Cho, H. Tahara, T. Yamada, H. Suzuura, T. Tadano, R. Sato, M. Saruyama, H. Hirori, T. Teranishi, and Y. Kanemitsu, Exciton–phonon and trion–phonon couplings revealed by photoluminescence spectroscopy of single cspbbr3 perovskite nanocrystals, *Nano Letters* **22**, 7674 (2022).

[23] Y. Guo, O. Yaffe, T. D. Hull, J. S. Owen, D. R. Reichman, and L. E. Brus, Dynamic emission stokes shift and liquid-like dielectric solvation of band edge carriers in lead-halide perovskites, *Nature Communications* **10**, 1175 (2019).

[24] C. M. Iaru, J. J. Geuchies, P. M. Koenraad, D. Vanmaekelbergh, and A. Y. Silov, Strong carrier–phonon coupling in lead halide perovskite nanocrystals, *ACS nano* **11**, 11024 (2017).

[25] P. Tamarat, E. Prin, Y. Berezovska, A. Moskalenko, T. P. T. Nguyen, C. Xia, L. Hou, J.-B. Trebbia, M. Zacharias, L. Pedesseau, C. Katan, M. I. Bodnarchuk, M. V. Kovalenko, J. Even, and B. Lounis, Universal scaling laws for charge-carrier interactions with quantum confinement in lead-halide perovskites, *Nature Communications* **14**, 229 (2023).

[26] L.-I. Bulyk, T. Demkiv, O. Antonyak, Y. M. Chornodolskyy, R. Gamernyk, A. Suchocki, and A. Voloshinovskii, Pressure influence on excitonic luminescence of cspbbr 3 perovskite, *Dalton Transactions* **52**, 16712 (2023).

[27] C. Zhu, L. G. Feld, M. Svyrydenko, I. Cherniukh, D. N. Dirin, M. I. Bodnarchuk, V. Wood, N. Yazdani, S. C. Boehme, M. V. Kovalenko, et al., Quantifying the size-dependent exciton–phonon coupling strength in single lead-halide perovskite quantum dots, *Advanced Optical Materials* **12**, 2301534 (2024).

[28] M.-R. Amara, Z. Said, C. Huo, A. Pierret, C. Voisin, W. Gao, Q. Xiong, and C. Diederichs, Spectral fingerprint of quantum confinement in single cspbbr3 nanocrystals, *Nano Letters* **23**, 3607 (2023).

[29] A. Ripin, R. Peng, X. Zhang, S. Chakravarthi, M. He, X. Xu, K.-M. Fu, T. Cao, and M. Li, Tunable phononic coupling in excitonic quantum emitters, *Nature Nanotechnology* **18**, 1020–1026 (2023).

[30] G. M. Anilkumar, M. Bhakar, C. Taneja, S. Hwang, G. V. P. Kumar, G. Sheet, and A. Rahman, Near room temperature solvothermal growth of ferroelectric cspbbr3 nanoplatelets with ultralow dark current, *Advanced Materials* **36**, 2403875 (2024).

[31] A. E. J. Hoffman, R. A. Saha, S. Borgmans, P. Puech, T. Braeckeveldt, M. B. J. Roeffaers, J. A. Steele, J. Hofkens, and V. Van Speybroeck, Understanding the phase transition mechanism in the lead halide perovskite cspbbr3 via theoretical and experimental giwaxs and raman spectroscopy, *Apl Materials* **11**, 2023.

[32] M. Bataev, M. Kuznetsova, D. Pankin, M. Smirnov, S. Y. Verbin, I. Ignatiev, I. Eliseyev, V. Y. Davydov, A. Smirnov, and E. Kolobkova, Electron–phonon interaction in perovskite nanocrystals in fluorophosphate glass matrix, *Semiconductors* **58**, 103 (2024).

[33] P. C. Sercel, J. L. Lyons, D. Wickramaratne, R. Vaxenburg, N. Bernstein, and A. L. Efros, Exciton fine structure in perovskite nanocrystals, *Nano letters* **19**, 4068 (2019).

[34] P. Tamarat, L. Hou, J.-B. Trebbia, A. Swarnkar, L. Biadala, Y. Louyer, M. I. Bodnarchuk, M. V. Kovalenko, J. Even, and B. Lounis, The dark exciton ground state promotes photon-pair emission in individual perovskite nanocrystals, *Nature Communications* **11**, 10.1038/s41467-020-19740-7 (2020).

[35] M. Fu, P. Tamarat, H. Huang, J. Even, A. L. Rogach, and B. Lounis, Neutral and charged exciton fine structure in single lead halide perovskite nanocrystals revealed by magneto-optical spectroscopy, *Nano Letters* **17**, 2895–2901 (2017).

[36] Z. Yang, A. Surrente, K. Galkowski, A. Miyata, O. Portugall, R. Sutton, A. Haghghirad, H. Snaith, D. Maude, P. Plochocka, et al., Impact of the halide cage on the electronic properties of fully inorganic cesium lead halide perovskites, *ACS Energy letters* **2**, 1621 (2017).

[37] K. Lin, X. Sun, F. Dirnberger, Y. Li, J. Qu, P. Wen, Z. Sofer, A. Söll, S. Winnerl, M. Helm, et al., Strong exciton–phonon coupling as a fingerprint of magnetic ordering in van der waals layered crsbr, *ACS nano* **18**, 2898 (2024).

[38] J. Kang and L.-W. Wang, High defect tolerance in lead halide perovskite cspbbr3, *The journal of physical chemistry letters* **8**, 489 (2017).

[39] M. Baranowski, S. J. Zelewski, M. Kepenekian, B. Traoré, J. M. Urban, A. Surrente, K. Galkowski, D. K. Maude, A. Kuc, E. P. Booker, et al., Phase-transition-induced carrier mass enhancement in 2d ruddlesden–popper perovskites, *ACS Energy Letters* **4**, 2386 (2019).

[40] A. Cohen, T. M. Brenner, J. Klarbring, R. Sharma, D. H. Fabini, R. Korobko, P. K. Nayak, O. Hellman, and O. Yaffe, Diverging expressions of anharmonicity in halide perovskites, *Advanced Materials* **34**, 2107932 (2022).

[41] X. Z. Du, J. Li, J. Y. Lin, and H. X. Jiang, Temperature dependence of the energy bandgap of multi-layer hexagonal boron nitride, *Applied Physics Letters* **111** (2017).

[42] L. V. Le, T. T. T. Huong, T.-T. Nguyen, X. A. Nguyen, T. H. Nguyen, S. Cho, Y. D. Kim, and T. J. Kim, The wannier-mott exciton, bound exciton, and optical phonon replicas of single-crystal gase, *Crystals* **14**, 539 (2024).

[43] L. Gao, L. Yadgarov, R. Sharma, R. Korobko, K. M. McCall, D. H. Fabini, C. C. Stoumpos, M. G. Kanatzidis, A. M. Rappe, and O. Yaffe, Metal cation s lone-pairs increase octahedral tilting instabilities in halide perovskites, *Materials Advances* **2**, 4610 (2021).

[44] J. Even, S. Thebaud, A. R. Kshirsagar, Z. Xu, L. Pedesseau, M. Zacharias, and C. Katan, *Theoretical approaches to fröhlich excitonic polarons in polar semiconductors* (2025), arXiv:2505.07406 [cond-mat.mtrl-sci].

[45] X. Li, S. Chen, P.-F. Liu, Y. Zhang, Y. Chen, H.-L. Wang, H. Yuan, and S. Feng, Evidence for ferroelectricity of all-inorganic perovskite cspbbr₃ quantum dots, *Journal of the American Chemical Society* **142**, 3316 (2020).

[46] D. Niesner, M. Wilhelm, I. Levchuk, A. Osvet, S. Shrestha, M. Batentschuk, C. Brabec, and T. Fauster, Giant rashba splitting in ch₃nh₃pbbr₃ organic-inorganic perovskite, *Physical review letters* **117**, 126401 (2016).

[47] P. R. Anandan, M. Nadeem, C.-H. Lin, S. Singh, X. Guan, J. Kim, S. Shahrokhi, M. Z. Rahaman, X. Geng, J.-K. Huang, H. Nguyen, H. Hu, P. Sharma, J. Seidel, X. Wang, and T. Wu, Spin-orbital coupling in all-inorganic metal-halide perovskites: The hidden force that matters, *Applied Physics Reviews* **10** (2023).

[48] Y. Wang, Y. Wang, T. A. Doherty, S. D. Stranks, F. Gao, and D. Yang, Octahedral units in halide perovskites, *Nature Reviews Chemistry* , 1 (2025).

[49] S. Krach, N. Forero-Correa, R.-I. Biega, S. E. Reyes-Lillo, and L. Leppert, Emergence of rashba-/dresselhaus effects in ruddlesden–popper halide perovskites with octahedral rotations, *Journal of physics: Condensed matter* **35**, 174001 (2023).

[50] M. Dyksik, Polaron vibronic progression shapes the optical response of 2d perovskites, *Advanced Science* **11**, 2305182 (2024).

[51] K. Posmyk, N. Zawadzka, Ł. Kipczak, M. Dyksik, A. Surrent, D. K. Maude, T. Kazimierczuk, A. Babiński, M. R. Molas, W. Bumrungsan, et al., Bright excitonic fine structure in metal-halide perovskites: from two-dimensional to bulk, *Journal of the American Chemical Society* **146**, 4687 (2024).

[52] X. Zhu, Large polarons in lead halide perovskites, *Science advances* **3**, e1701217 (2017).

[53] T. Lanigan-Atkins, X. He, M. J. Krogstad, D. M. Pajerowski, D. L. Abernathy, G. N. M. N. Xu, Z. Xu, D.-Y. Chung, M. G. Kanatzidis, S. Rosenkranz, R. Osborn, and O. Delaire, Two-dimensional overdamped fluctuations of the soft perovskite lattice in cspbbr₃, *Nature materials* **20**, 977 (2021).

[54] J. Lahnsteiner, M. Rang, and M. Bokdam, Tuning einstein oscillator frequencies of cation rattlers: A molecular dynamics study of the lattice thermal conductivity of cspbbr₃, *The Journal of Physical Chemistry C* **128**, 1341 (2024).

[55] X. Ma, P. Shen, Y.-N. Wang, F. Pan, G. Chen, S. Xu, and H. Ye, Local phonon modes concerned with the self-trapped exciton state in cspbbr₃ nanocrystals, *The Journal of Physical Chemistry C* **124**, 27130 (2020).

[56] G. Antonius and S. G. Louie, Theory of exciton-phonon coupling, *Phys. Rev. B* **105**, 085111 (2022).